Title

Intracellular imaging of metmyoglobin and oxygen using new dual purpose probe EYFP-Myoglobin-mCherry.

Journal

Journal of Biophotonics, 15(3)

Authors

Penjweini, Rozhin
Roarke, Branden
Alspaugh, Greg
et al.

Publication Date

2022-03-01

DOI

10.1002/jbio.202100166

Peer reviewed

HHS Public Access

Author manuscript

J Biophotonics. Author manuscript; available in PMC 2023 March 01.

Published in final edited form as:

J Biophotonics. 2022 March ; 15(3): e202100166. doi:10.1002/jbio.202100166.

Intracellular *imaging* of metmyoglobin and oxygen using new dual purpose probe EYFP-Myoglobin-mCherry

Rozhin Penjweini[a], **Branden Roarke**[a], **Greg Alspaugh**[a], **Katie A. Link**[a], **Alessio Andreoni**[a,b], **Mateus P. Mori**[c], **Paul M. Hwang**[c], **Dan L. Sackett**[d], **Jay R. Knutson**[a,*]

[a]Laboratory of Advanced Microscopy and Biophotonics, National Heart, Lung, and Blood Institute (NHLBI), National Institutes of Health (NIH), Bethesda, MD 20892-1412.

[b]Laboratory of Optical Neurophysiology, Department of Biochemistry and Molecular Medicine, University of California Davis, Tupper Hall, Davis, CA 95616.

[c]Laboratory of Cardiovascular and Cancer Genetics, NHLBI, NIH, Bethesda, MD 20892-1412.

[d]Cytoskeletal Dynamics Group, Division of Basic and Translational Biophysics, Eunice Kennedy Shriver National Institute of Child Health and Human Development, NIH, Bethesda MD, 20892-0924.

Abstract

The biological relevance of nitric oxide (NO) and reactive oxygen species (ROS) in signaling, metabolic regulation and disease treatment has become abundantly clear. The dramatic change in NO/ROS processing that accompanies a changing oxygen landscape calls for new imaging tools that can provide cellular details about both [O_2] and the production of reactive species. Myoglobin oxidation by NO/ROS to the *met* state is a known sensor with absorbance changes in the visible range. We previously employed Förster resonance energy transfer (FRET) to read out the deoxygenation/oxygenation of myoglobin, creating the subcellular [O_2] sensor Myoglobin-mCherry. We now add the fluorescent protein EYFP to create a novel probe that senses **both** *met* formation, a proxy for ROS/NO exposure, and [O_2]. Since both proteins are present in the construct, it can also relieve users from the need to measure fluorescence lifetime, making [O_2] sensing available to a wider group of laboratories.

Graphical Abstract

*Correspondence: knutsonj@nhlbi.nih.gov; Tel: +1 (301) 496-2557; fax: +1 (301) 480-6964.

DATA AVAILABILITY STATEMENT

The data that support the findings of this study are available from the corresponding author upon reasonable request.

SUPPORTING INFORMATION

Additional supporting information is available in the online version of this article at the publisher's website or from the author. Extended detail of interactions of different states of myoglobin with NO; calculated FRET efficiency and lifetime for EYFP-Myoglobin and EYFP-Myoglobin-mCherry; EYFP-Myoglobin sensor; time-course reduction of metmyoglobin in A549 cells; Detection of probable NAD(P)H-dependent cytochrome b_5 reductase activity; mCherry moiety retains oxygen sensing: detection of [O_2] using fluorescence lifetime imaging of mCherry in Myoglobin-mCherry and EYFP-Myoglobin-mCherry sensors; Time-course changes in the EYFP and mCherry fluorescence emission of the FRET sensor in A549 cells.

CONFLICTS OF INTEREST

The authors declare no potential conflict of interest.

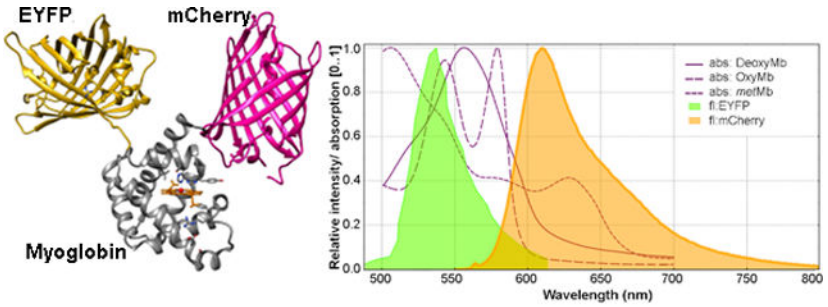

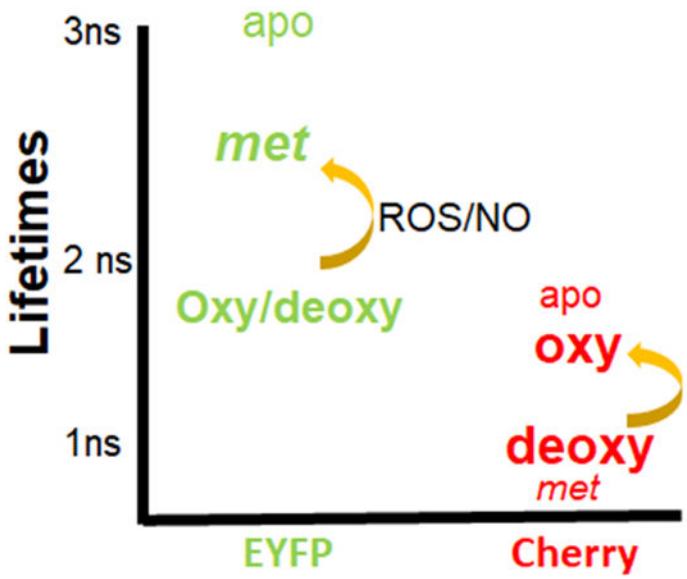

Keywords

EYFP-Myoglobin-mCherry; FLIM; *met*Mb; NO; ROS

1 | INTRODUCTION

Intracellular oxygen concentration ([O_2]) affects the oxidation/reduction properties of signaling proteins and enzymes, influencing the levels of nitric oxide (NO) and reactive oxygen species (ROS) [1,2]. At normal oxygen (O_2) partial pressure in the lung (normoxia; pO_2 ~ 100 mmHg) and physiological O_2 levels (physioxia; pO_2 ~ 20–40 mmHg), NO and ROS are generally produced at minimal levels and act as critical signaling molecules subject to a dedicated balance between their production and elimination [1,3]. It has been demonstrated that increased NO and ROS concentration ([NO] and [ROS]) can also be a contributing factor to hypoxia-inducible factor stabilization during hypoxia and reoxygenation [4]. However, when [NO] and [ROS] exceed depletion mechanisms, they can cause oxidative stress with deleterious consequences including cancer and cardiovascular disease [1,5]. Thus, the role of NO/ROS in health and disease is related to production rates, steady-state concentrations, and disposal mechanisms that modulate their activity [4,6]. Although clinical intervention into these mechanisms continues to attract research interest,

the measurement of real-time *in vivo* levels of NO, ROS and O_2 remains a significant challenge. New techniques are needed to simultaneously and noninvasively monitor cellular NO, ROS and O_2; such methods may facilitate the pursuit of novel therapies.

We previously introduced a Förster resonance energy transfer (FRET)-based probe, myoglobin-mCherry, for monitoring [O_2] [7,8]. This sensor was based on using donor (mCherry) lifetime sensitivity to spectral changes in myoglobin absorbance to discriminate oxygenated myoglobin (OxyMb) from deoxygenated myoglobin (DeoxyMb) within a chimeric construct. In the present study, we introduce a genetically encoded sensor, EYFP-Myoglobin-mCherry, that still permits [O_2] monitoring while, importantly, enabling us to observe the formation of metmyoglobin (*met*Mb) as a marker of oxidative stress - while minimally perturbing the endogenous landscape. As reported previously [9], fluorescent chimeras are likely expressed at sub micromolar levels and are thus unlikely to change O_2 buffering, diffusion, or NO/ROS equilibria. Our EYFP-Myoglobin-mCherry sensor works by measuring FRET from **either** EYFP or mCherry to myoglobin, and the *met*- and O_2-dependent absorbance of that acceptor is thus revealed in their independent fluorescence.

[O_2] and reduced-nicotinamide adenine dinucleotide (phosphate)[H] (NAD(P)H)-dependent *met*/free radical reducing activity are two essential biochemical influences upon OxyMb, DeoxyMb, and *met*Mb proportions [10,11]. In cells replete with myoglobin (e.g. myocytes), rapid oxidation of NO by OxyMb occurs under normoxia with the formation of nitrate (NO_3^-) and *met*Mb (heme iron in the ferric state (Fe^{3+})) [12,13]. This is also induced by strong oxidizing agents such as ROS or while myoglobin clears NO/ROS for cell protection [12,13]. Under hypoxia, the interaction of DeoxyMb with nitrite (NO_2^-) might also be of relevance for NO generation [2,14,15]. The *met*Mb state could also form via nitrosylation of DeoxyMb, (see Supporting Figure S1) [12,16]. The processes in low-myoglobin cell types may be very different, however; the concentration of *met*Mb in *most* cells is usually low due to the NAD(P)H-dependent cytochrome b_5 reductase clearance of *met*/free radicals (as well as the low expression of myoglobin in most cells) [10].

To demonstrate the utility of this EYFP-Myoglobin-mCherry sensor, we measure EYFP lifetime and quantify the *met*-form accumulation seen with ROS or NO treatment at various imposed [O_2] in A549 human non-small-cell lung cancer cells. We correlate our observed *met*Mb readout with the levels of NO/ROS generated in several conditions: in hypoxia, in treatment with defined exogenous quantities of S-nitrosoglutathione (a NO donor denoted as ‘SNOG’), exposure to illuminated TOOKAD® WST11 (a radical generating type I photosensitizer), and treatment with mito-TEMPO (a mitochondria-targeted ROS scavenger). The second and independent feature of the probe, [O_2] quantitation, is also shown by the intensity ratio of EYFP/mCherry. Metabolic insights from the contemporaneous fluorescence lifetime imaging (FLIM) of free and enzyme-bound NAD(P)H pools are added for context.

2 | WORKING PRINCIPLE OF THE EYFP-MYOGLOBIN-MCHERRY PROBE

EYFP-Myoglobin-mCherry is a FRET-based probe that was constructed by expressing as a chimera (N-term to C-term): the yellow fluorescent protein EYFP, myoglobin and the red

fluorescent protein mCherry (see Figure 1A). The myoglobin picked for this probe has low pH/ion sensitivity and the analyte endpoints were designed to match real environments. As shown in Figure 1B, the absorption spectra of myoglobin in 500–630 nm and 550–700 nm regions overlap with the emissions of EYFP and mCherry, respectively [17,18]. FRET can thus occur to myoglobin (non-fluorescent acceptor) from either the yellow or red fluorescent proteins (donors). Using spectral data for EYFP, myoglobin and mCherry with extinction coefficients of the proteins, the Förster radius (R_0) for the Oxy, Deoxy or *met* forms can be (approximately) estimated (see Supporting Table S1) [8]. Characterization and evolution of similar FRET probes for live cells and tissues are ongoing and will be presented in another study. Biophysical characterization of the purified probe *in vitro* (e.g. extrapolated binding, kinetics and distance information of the sensor alone) goes beyond the scope of this manuscript, but more detailed calculations on these FRET systems are available [19,20].

In the combined EYFP-Myoglobin-mCherry sensor, changes in myoglobin spectral features with O_2 occupancy or upon *met*Mb production control the amount of energy transferred **from** the fluorescent proteins **to** myoglobin. The greater overlap (highlighted by shaded areas) creates greater transfer rates. As shown in Figure 1C (shaded area), when O_2 is bound, mCherry fluorescence is only slightly quenched, and when *either* O_2 is released or *met* is produced, FRET will increase- and this reduces both yield and lifetime [7,8]. Unlike mCherry, the EYFP fluorescence moiety is sensitive to *met*Mb and **not** [O_2], because FRET rates to Oxy and Deoxy are very similar in this emission color band; this was further confirmed by intensity and FLIM of EYFP in a simpler EYFP-Myoglobin dimeric construct (i.e. without mCherry) (see Supporting Figure S2). The intracellular fluorescence mean lifetime of EYFP alone is ~ 3.1 ns [21,22]. Assuming that mCherry and EYFP chromophores are kept > 5 nm apart by the myoglobin interposed between them, the lifetime of ***both*** EYFP-OxyMb and EYFP-DeoxyMb are predicted to be the same and just below 2 ns, since the R_0 for FRET between EYFP and Deoxy vs. Oxy differs by less than 0.06 nm (see Supporting Table S1). This yellow emission lifetime should, however, increase significantly in the presence of *met*Mb, with less spectral overlap with EYFP, and thus a shorter R_0 (see lesser shaded area in Figure 1D). Gathering these responses together, imaging the **EYFP/mCherry intensity ratio will reveal the intracellular [O_2]** while **FLIM of EYFP emission monitors *met*Mb**. The FRET probe ratio for O_2 would, of course, need second order algebraic correction for significant *met*Mb levels, if present.

Like all fluorescent protein sensors, our chimera might experience unanticipated novel interactions within cells that interfere with the sensor function. To that end, we have taken great care to design the probes to insulate the measurement from artifacts one might reasonably anticipate such as index of refraction changes, chromophore maturation differences, hemolysis, and denaturation. In this study, we benchmark reversible changes in the O_2 parent chimera (Myoglobin-mCherry) [7,8] and address the main selectivity issue (*met*Mb vs. DeoxyMb) by making a “sandwich” version with EYFP.

3 | MATERIALS AND METHODS

3.1 | EYFP-Myoglobin and EYFP-Myoglobin-mCherry preparation

The pmCherry N1 vector (Clonetech, Mountain View, California, US) was used as a template to introduce the myoglobin gene (*Physeter catodon*, Sperm Whale, Addgene Plasmid pMB413a, #20058) at the C-terminus of mCherry. EYFP was a kind gift from Philippe Cluzel (Addgene plasmid pEB1-mEYFP, #103985) [23]. A very short (2-residue) glycine-serine linker was inserted between EYFP and myoglobin, and between myoglobin and mCherry to allow for limited flexibility (a measure that, coupled with the depolarized acceptor symmetry, reduces FRET orientation change effects) yet prevents misfolding [24]. Cloning was performed using the In-Fusion molecular cloning kit (Takara Bio, Mountain View, CA, US) according to the instructions from the manufacturer. Expression in eukaryotic cells is obtained via the CMV promoter and enhancer originally present in the pmCherry N1 plasmid used as a template. Sequences of the final products were verified via Sanger sequencing.

3.2 | Cell transfection

A549 cells were kept in Modified Eagle's Medium (DMEM, Gibco, Grand Island, NY, US) combined with 10% fetal bovine serum (FBS), and 1% penicillin-streptomycin (Mediatech Inc. Manassas, VA, US). The cells were plated in μ-Slide 4- or 8- well chambers (Ibidi GmbH, Martinsried, Germany) with a density of 2×10^4 cells/cm^2. To transfect cells with EYFP, EYFP-Myoglobin or EYFP-Myoglobin-mCherry, plasmid DNA diluted in 1000 μL of Opti-MEM® medium (Gibco) was combined with 3 μL of Lipofectamine® 2000 transfection reagent (Invitrogen, Carlsbad, CA, US) diluted in 1000 μL of Opti-MEM. After a 15-min period, the DNA-Lipofectamine transfection complex was added to the cells with a final plasmid concentration of 2.5 ng/μL. After 32 h incubation at 37°C and 5% CO_2, the transfection media was removed, and the cells were washed and covered with fresh cell medium.

3.3 | Transfection efficiency and cytotoxicity measurements

A total of at least 15 images for yellow/red channels and phase contrast (covering a surface area of 676 × 676 μm^2) were acquired using a Zeiss LSM 780 confocal microscope (Carl Zeiss, Germany) equipped with an air 20× objective, 48 h after the cell transfection. EYFP and mCherry were excited by Argon 514 nm and diode 594 nm lasers, and the emission was collected in separate photon-counting channels using adjustable bandpass filters of 517–606 nm and 614–686 nm. CellProfiler image analysis software [25] was used to determine the total area covered by cells in phase, and yellow/red channels. Transfection efficiency was expressed as the percentage of the area covered by transfected cells over the total area covered by cells measured in phase contrast; control cells were treated with Lipofectamine only (no plasmid). For cytotoxicity measurements, the cells from each well were stained with Trypan Blue (in a 1:10 dilution) and 1 μg/ml Hoechst 33342 (Molecular Probes, Eugene, OR, USA) for 30 min. Then, a total of 5 images for phase and blue channels (covering a surface area of 676 × 676 μm^2) were acquired to count the viable and total cell number. Hoechst was excited by a diode 355 nm laser and the emission was collected using an adjustable bandpass filter of 499–606 nm.

3.4 | NO generation using SNOG

For modulation of *met*Mb, SNOG (Tocris Bioscience, Minneapolis, MN, USA) was used to release known quantities of NO into cell culture media [26]. On the day of imaging, SNOG solutions of varying concentrations were prepared by diluting 1 mM stock solution (DMEM without FBS was used as a solvent) with additional DMEM. Cell media was removed from the cell chambers and replaced with the desired SNOG solution, followed by imaging. SNOG concentrations used include, 3, 50, 100, 250, and 350 μM; higher concentrations showed cytotoxicity especially at hypoxia.

3.5 | Modulation of ROS using TOOKAD and mito-TEMPO

TOOKAD solutions of 5, 10, 50 and 100 nM were prepared by diluting 1 mM stock solution (dimethyl sulfoxide (DMSO) was used as a cosolvent) with DMEM without FBS. The mito-TEMPO stock solution (1 mM prepared with pure water) was diluted in culture medium to the final concentrations of 1, 5, 10 and 25 μM. One hour before imaging, the plated cells were treated with TOOKAD or mito-TEMPO in the dark at 37°C and 5% CO_2 for modulation of *met*Mb. Consistent illumination exposures were applied to each TOOKAD experiment for ROS generation.

3.6 | Inhibition of NADH cytochrome b_5 reductase or mitochondrial O_2 consumption

For inhibition of *met*Mb reductase or mitochondrial O_2 consumption, A549 cells were treated with 40 μM propylthiouracil (PTU) or a mixture of 2 μM rotenone/antimycin A (Millipore SIGMA, Burlington, MA, USA), respectively. PTU inhibits *met*Mb reductase or NADH cytochrome b_5 reductase 3 (CYB5R35: NADH: ferricytochrome b_5 oxidoreductase, EC1.6.2.2), which is a critical flavoprotein for NO signaling and it transfers electrons from the NADH domain of CYB5R3 to cytochrome b_5 [27]. Rotenone inhibits the transfer of electrons from complex I to co-enzyme Q (CoQ), whereas antimycin A prevents the oxidation of CoQ by cytochrome *c*.

3.7 | Microscopic visualization of carbonyl formation in the intracellular environment

For detection of carbonyl groups induced by oxidative or nitrative stress, A549 cells were treated with various TOOKAD and SNOG concentrations for 1 h at 37 °C, 5% CO_2 and 20%, 10% or 0.5% O_2; TOOKAD was excited with 740 nm at the end of the incubation. Then, the cells were incubated with 10 μM BODIPY™ FL Hydrazide (4,4-Difluoro-5,7-Dimethyl-4-Bora-3a,4a-Diaza-s-Indacene-3-Propionic Acid, Hydrazide) for detecting carbonyl groups [28], and 1 μg/ml Hoechst for detecting the nucleus during image processing; DMSO was used as a cosolvent for the probes in medium. After 1 h incubation at 37 °C and 5% CO_2, cells were washed with fresh media at least three times for 3 min and were imaged using the Zeiss LSM780 confocal microscope.

3.8 | Griess reagent for NO determination in the cell media

The Griess reagent kit (Molecular Probes, Eugene, OR, USA) was used to detect NO in cell media at various SNOG concentrations with a lower detection limit of 2.5 μM as specified by the manufacturer. Briefly, different concentrations of SNOG were prepared in the media and equal volumes of sulfanilic acid and N-(1-naphthyl) ethylenediamine were

added to the samples sequentially every 5 min. A reference curve with the Griess Nitrite Standard was also prepared, using the same media at the same SNOG concentrations. The absorbances of all samples in the range of 400–680 nm were measured using a Cary 60 UV/Vis spectrophotometer (Agilent Technologies, Santa Clara, CA, USA). Finally, the SNOG absorbances were converted to [NO] using the Griess Standard curve as described by the manufacturer.

3.9 | Imaging systems

Two-photon FLIM was performed using an Olympus IX81 confocal laser scanning microscope (Melville, NY, USA) equipped with a tunable Mai Tai BB DeepSee femtosecond laser (Spectra-Physics, Santa Clara, CA, USA) operating at 80 MHz, with wavelengths set to 900 nm for the excitation of EYFP or 740 nm for the excitation of NAD(P)H and mCherry; both 900 and 740 nm can excite TOOKAD. The laser light was passed through a 690 nm dichroic mirror and directed to an Olympus UPLANSAPO 60×, 1.2 NA water immersion objective. The emission was directed to the side port of the microscope (non-descanned detection) and passed through a 675 nm short pass filter to reduce scattered light. The EYFP, mCherry and NAD(P)H signals were filtered through 520/60 nm, 647/57 nm and 460/60 nm bandpass filters (Semrock BrightLine®, Rochester, NY, US), respectively. The fluorescence was focused on a PMC100 cooled detector (Becker & Hickl GmbH, Berlin, Germany) and the electrical pulse output from the detector was directed into an SPC-150 photon counting card (Becker & Hickl). The signals were synchronized with the pulses from the laser to allow for time-correlated single photon counting (TCSPC). Synchronization with the pixel, line, and frame clock from the scanning unit of the microscope was used for image construction in TCSPC mode. The cells were excited with a laser power ≤18 mW and imaged for 40–80 s to accumulate an adequate number of photons per pixel and to avoid photobleaching and photocytotoxicity. Image size was set to 256 × 256 $(\text{pixels})^2$, and TCSPC histograms were collected with 256 channels in a 12.5 ns time window. To avoid intermolecular FRET, low signal to noise ratio for the two lifetimes, or effects of pH and refractive index on the lifetime values, we did not image rare cells showing unusually high or low signals or with a punctate fluorescence pattern. Selection criteria are further discussed in Ref. [29].

General fluorescence microscopy images (including EYFP/mCherry intensity ratio) were collected using the Zeiss LSM 780 confocal microscope equipped with a Plan-Apochromat 63×/1.4 NA Oil immersion objective. Hoechst, BODIPY FL Hydrazide, EYFP and mCherry were excited by diode 355 nm, Argon 488 nm, diode 514 nm and diode 594 nm lasers, respectively. The fluorescence was directed toward two Photomultiplier Tubes (PMT), and it was spectrally filtered by an adjustable bandpass filter in photon-counting mode set to 437–473 nm for Hoechst, 499–526 nm for BODIPY, 517–535 nm for EYFP and 597–615 nm for mCherry. For EYFP/mCherry intensity ratio measurements, single cells were imaged using the aforementioned criteria. For the samples treated with Hoechst and BODIPY, the fluorophores were imaged simultaneously in separate detection channels, and samples were acquired using a 5 × 5 tiling procedure (25 total 135 × 135 μm images) covering a surface area of 0.457 mm^2 in each well. The individual frames were acquired with a pixel size in the range of 0.05–0.10 μm and a pixel dwell time of 1.58 μs.

3.10 | Controlling imposed O_2 during imaging

A miniature incubator was mounted on the microscope stage and connected to a gas mixing system (CO_2−O_2−MI, Bioscience Tools, San Diego, CA) to deliver mixtures of N_2, O_2, and CO_2 inside the chamber according to the inputs set by the user. During the live cell imaging, the incubator kept the temperature at 37°C, maintained CO_2 at 5% and set O_2 at different concentrations from 20 to 0.5%; 0.5% is the lowest $\%O_2$ reachable by our system. The cell culture (in dishes with a ~3 mm layer of medium above cells, without lids) reaches a stable $\%O_2$ within 30 min.

3.11 | FLIM analyses

FLIM data were analyzed using the SPCImage software (Becker & Hickl). The decay curves at each pixel were fit using a least-square method to follow a double-exponential decay model:

$$F(t) = a_1 exp(-t/\tau_1) + a_2 exp(-t/\tau_2) \quad (1)$$

where a_1 and a_2 are the pre-exponential factors and can be used (if natural lifetime is constant) to represent the fraction of fluorophores with lifetimes τ_1 and τ_2, respectively. The mean lifetime (τ_{mean}) is calculated from these amplitude weighting parameters as well.

Fitting was performed via iterative reconvolution with a default synthetically generated Instrument Response Function (IRF). The lifetime decay values were obtained by a multi-exponential model in SPCImage at optimized goodness of fit (χ^2) [7]. Binning of adjacent pixels was used (setting: 5–8) to avoid fitting decays with a peak count lower than 1000. In the cells treated with SNOG, TOOKAD or mito-TEMPO, the EYFP lifetime was calculated by taking τ_{mean} from each single image and averaging this across multiple cells (n > 30). Then, the full image averaged values of EYFP lifetime, taken for multiple cells, were correlated to the drug concentration by the Curve Fitting Toolbox in MATLAB R2020a (The MathWorks Inc., Natick, MA, USA). The relationship between the EYFP lifetime in the FRET sensor and SNOG or TOOKAD concentration was found to be approximately hyperbolic. A full set of parameters including τ_1, τ_2, $a_1\%$, $a_2\%$, normalized a_1 and a_2 ($|a_1|$ and $|a_2|$) for NAD(P)H were also generated. Finally, color-mapped lifetime images of EYFP and free/bound NAD(P)H distribution were obtained for each cell.

3.12 | Fluorescence intensity and ratio analyses

BODIPY FL Hydrazide and Hoechst signals were pre-processed using a custom ImageJ macro, analyzed using the CellProfiler software, and post-processed using a custom MATLAB R2020a (The MathWorks Inc.) script. Briefly, individual nuclei were identified from the Hoechst channel followed by identification of their parent cells from the BODIPY FL Hydrazide channel using an improved watershed algorithm. The integrated intensity of each cell was measured from the BODIPY FL Hydrazide signal.

For the correlation of $O_2\%$ to the EYFP/mCherry intensity ratio, the yellow and red signals were pre-processed using custom ImageJ macros, analyzed using CellProfiler, and post-processed using a custom MATLAB script. The integrated intensity of each cell

was measured from both the EYFP and mCherry channels. A MATLAB script provided pseudocolor mapping of the ratio.

3.13 | Statistical analyses

At least three independent experiments were performed for each imaging; the mean values are presented with standard deviation or standard error of the mean. Kruskal-Wallis or Mann-Whitney U tests were used to evaluate whether the values in the independent groups are significantly different from each other. Analyses were carried out using SPSS 14.0 software (IBM, Chicago, Illinois, USA) and statistical significance was defined at $p < 0.05$ (95% confidence level).

4 | RESULTS AND DISCUSSION

4.1 | Detection of NO and ROS sequelae upon SNOG and TOOKAD treatment

Oxidative modification of proteins by excessive ROS mainly affects side chains, with carbonyl groups being among the products [28]. Detection of carbonyl groups has become an accepted method for measuring oxidative protein damage. We quantified BODIPY FL Hydrazide [28] fluorescence in the cells treated with TOOKAD and SNOG to explore the formation of carbonyl groups. Cells labelled with BODIPY FL Hydrazide but no other treatments were used as controls.

As expected, exposure to TOOKAD caused a significant dose-dependent increase in carbonyl groups (see Figure 2A). As TOOKAD concentration increased to 100 nM and/or imposed O_2 decreased to 10 or 0.5%, the formation of carbonyl groups increased to a maximum. Mann-Whitney tests did not show a significant difference between the results for imposed O_2% of 10 and 0.5 in all possible pairwise combinations (p-value ≥ 0.65).

Although several mechanisms of NO-mediated cytoprotection against oxidative stress are known during hypoxia [30], our results show increases in the formation of carbonyl groups in cells treated with SNOG at all imposed O_2%. A precedent exists for nitrosative stress, where formation of carbonyl groups and nitration in HT22 mouse hippocampal neuronal cells paralleled each other [31]. As shown in Figure 2B, the formation of carbonyl groups increased with SNOG concentration or decrease of imposed O_2%; results for imposed O_2% of 10 and 0.5 were not statistically different (Mann-Whitney p-value ≥ 0.70). Additionally, the ability of SNOG to generate NO in the cell culture media was evaluated using the Griess Reagent. As shown in Figure 2C, to generate the NO standard reference curve, the average absorbance value was plotted as a function of imposed [NO] (see Figure 2D). Then, SNOG induced [NO] in the media were obtained from the standard curve. The results show [NO] of 4, 101, 221, 654 and 915 μM corresponding to SNOG 3, 50, 100, 250 and 350 μM, respectively.

4.2 | First probe function: detection of metMb using lifetime imaging of EYFP in the FRET sensor

*met*Mb can form due to a rapid oxidation of NO by OxyMb or by nitrosylation of DeoxyMb at hypoxia, yielding MbNO as an intermediate [12]. The presence of the enzyme *met*Mb/free

radical reductase (mainly NAD(P)H-dependent coenzyme cytochrome b_5) usually means the *met*Mb level in living cells is likely to be small [10,16,32]. To monitor *met*Mb formation and reductase effects, we expressed EYFP-Myoglobin-mCherry in the cytoplasm of A549 cells. Transient transfection of this newly developed sensor showed an efficiency of 20.5 % ± 7.2%, with no significant sign of cytotoxicity or changes in growth behavior as compared to the control with no transfection (Kruskal-Wallis p value = 0.37). We performed lifetime imaging on cells expressing the probe at different imposed O_2% (from 20 to 0.5) and used the lifetime of EYFP as a direct reporter of *met*Mb.

As shown in Figures 3A and B, NO application resulted in an increased EYFP lifetime (in both normoxia and hypoxia). This is due to the conversion of (higher FRET equivalent states) OxyMb and DeoxyMb to (lower FRET state) *met*Mb. SNOG produced a concentration-dependent increase of EYFP lifetime, showing hyperbolic behavior (see Figure 3B). The unknown, but potentially dominant, effects of *met*Mb reductase (e.g. NAD(P)H-dependent cytochrome b_5 reductase) may protect well-oxygenated cells [33], because FLIM gave no evidence for any *met*Mb formation in the cells under moderate NO challenges (< 3 μM). Nonetheless, it should be noticed that at higher NO doses (i.e. those sufficient to completely convert myoglobin to *met*Mb), any such restraint was clearly overwhelmed. The asymptotic maximum lifetime increase was observed following 350 μM SNOG treatment, when the probe lifetime increased by 35, 34 and 38% at the imposed O_2 of 20, 10 and 0.5%, respectively; cells incubated without SNOG were used as a control. As an aside, a slow post-washout decrease of EYFP lifetime, possibly due to intrinsic *met* reductase activity, is shown in Supporting Figure S3.

In the next step, we correlated *met*Mb generation with the levels of free radicals in cells subjected to TOOKAD vs. mito-TEMPO treatment. Excitation of TOOKAD with a wavelength in the near-infrared region generates reactive nitrogen species and especially ROS in the form of superoxide, hydroxyl radicals and hydrogen peroxide (H_2O_2) [34,35]. The oxidation of ferrous-OxyMb to ferric-*met*Mb occurs in the presence of ROS [36]. Ferric *met*Mb reacts with H_2O_2, which can be decomposed by *met*Mb via the cyclic formation of the ferryl species and tyrosine radicals [37–39]. Myoglobin can cause decomposition of H_2O_2, via the ferry1 species and this may vary depending on ambient [O_2] [36,37]. Myoglobin might help protect some cells against peroxides.

Herein, we examined the dose-response relationship between ROS and *met*Mb formation. The changes of EYFP lifetime that reveal *met* form were measured vs. ROS dosage/exposure (via sensitizer) at imposed [O_2] of 20, 10 and 0.5%. Based on the results shown in Figure 3B, TOOKAD sensitizer treatment increased lifetime values by 38, 34 and 37%. A hyperbolic relationship was observed between EYFP lifetime and the TOOKAD concentration. Scavenger mito-TEMPO, in contrast, did not have any significant impact on the lifetime values of EYFP in the FRET sensor (Kruskal-Wallis p-value ≥ 0.07).

As shown in Figure 3B (in the right panel), EYFP control (alone, lacking a *met* sensing moiety) lifetime is insensitive to intracellular *met*Mb, either from ROS or NO (Kruskal-Wallis p-value ≥ 0.07). This allows us to confirm that, on average, unrelated intracellular environmental variables such as refractive index or temperature have a negligible effect

on the fluorescence lifetime of EYFP (when compared to the effect exerted by the *met*Mb-sensing domain).

The potential, unknown role of cytochrome b_5 reductase in A549 cells was investigated next in a semi-quantitative way. We measured EYFP lifetime in cells treated with reductase inhibitor PTU; cells without PTU but treated with SNOG or TOOKAD were compared. As shown in Figure 3C, EYFP lifetime still increased above controls in the PTU-treated cells due to *met*Mb accumulation. The increase in EYFP lifetime due to the inhibition of cytochrome b_5 reductase was, however, statistically significant in cells treated with none or 3 μM SNOG. A possible explanation for the lack of response to PTU at higher concentrations than these might be due to the dominance/saturation of *met* production from NO/ROS at levels too high for reductase detoxification. In other words, the PTU inhibition effect (a measure of the reductase activity) is small compared to the *met*Mb generation rate at 100 μM or higher SNOG. As the effects of PTU on SNOG and TOOKAD treated cells were essentially the same, Figure 3C only presents the results for SNOG. Lifetime imaging of NAD(P)H autofluorescence at different imposed O_2% was additionally employed to investigate how cytochrome b_5 reductase regulates cellular response under stressed conditions (see Supporting Figure S4). FLIM can determine the changes of free (a_1, mainly in cytoplasm) and enzyme-bound (a_2, majority in mitochondria) NAD(P)H pools in response to the stressors and inhibition of the cytochrome b_5 reductase.

4.3 | Second probe function: detection of O_2 changes using intensity ratio of EYFP/mCherry in the FRET sensor

We previously showed [O_2] changes can be monitored using the sensitivity of the mCherry lifetime to spectral overlap changes in the absorbance of OxyMb and DeoxyMb either in chimera [7] or within the dual FRET sensor EYFP-Myoglobin-mCherry (see Supporting Figure S5). FLIM has many advantages over ratiometric microscopy, and we **prefer** quantifying both *met* and [O_2] with FLIM when possible. For example, FLIM nullifies concentration/loading issues (to at least first order) and quantifies the oxygenation levels in an intensity-independent manner. Since FLIM is not available in many facilities, however, we show here that the emission intensity ratio of EYFP/mCherry (O_2 insensitive/sensitive readouts) can also detect [O_2] changes. This allows the use of our sensor on any confocal microscope equipped to detect two emission channels, without requiring specialized FLIM detection equipment. Figure 4 shows the changes of intensity ratio EYFP/mCherry in response to different imposed O_2% (from 20 to 0.5); the intensity ratios for all O_2% were measured using an identical imaging setup. The method relies on both chromophores maturing and degrading as a unit; the minor time-course changes of EYFP and mCherry intensity in the many hours after transfection are shown in Supporting Figure S6.

As expected, the intensity ratio of EYFP/mCherry increased with decreasing imposed O_2%. To evaluate the effect of *mitochondrial* O_2 consumption on observed EYFP/mCherry intensity ratio, fluorescence imaging of the cells treated with a mixture of complex I and III inhibitors, rotenone and antimycin A, was performed. The results show that the inhibition of *mitochondrial* O_2 consumption **increased** net intracellular [O_2] (eliminated a sink) and thus decreased EYFP/mCherry intensity ratios at all imposed [O_2]. These measurements can

be directly compared to similar calibrations in our prior FLIM use of myo-mCherry [7,8], although (inverse) intensity and molecular mean -derived lifetime curves must, by definition, differ somewhat.

5 | CONCLUSION

In this study, we introduced EYFP-Myoglobin-mCherry, a probe that allows us to simultaneously quantify the intracellular accumulation of *met*Mb (via lifetime imaging of EYFP) and *also* serve to report [O_2] via the intensity ratio of EYFP/mCherry. Given the well-documented ability of myoglobin to scavenge free radicals through an intermediate state of *met*Mb [37], we examined *met*Mb induction vs. nitrative/ oxidative stress. We correlated *met*Mb generation with NO and ROS levels in A549 cells subjected to hypoxia, to treatment with SNOG (a NO donor), TOOKAD (a radical generating photosensitizer), and mito-TEMPO (a ROS scavenger). The increased lifetime of the EYFP portion of the probe showed *met*Mb was produced from either OxyMb or DeoxyMb upon treatment with SNOG and TOOKAD. Separately, we showed that the intensity ratio of EYFP/mCherry tracks media-imposed O_2%. Since *met*Mb is subject to NAD(P)H-dependent restoration activity, we crudely examined the role of poisoning cytochrome b_5 reductase. To show that our probe does not interfere with metabolic imaging, we also monitored the consequences of *met*Mb/ free radical reductase activity by FLIM investigation of free and enzyme-bound NAD(P)H pools. Based on our results, free and bound NAD(P)H both depleted under nitrative/ oxidative stress. Inhibition of cytochrome b_5 reductase yielded significantly higher levels of free NAD(P)H and thus ‘more glycolytic’ metabolism and less oxidative phosphorylation (see these peripheral results in Supporting Figure S4). This is in agreement with a previous study that reports increased mitochondrial function and lower levels of oxidative/nitrative damage in cells overexpressing cytochrome b_5 reductase [40].

Although myoglobin is not globally expressed in all cells, it has recently been found to be overexpressed in some types of cancer cells. It has been acknowledged, though, that *met*Mb might have a broad functional role in metabolic pathways, oxidative/nitrative regulation and gene networks of some epithelial cancer cells [41]. Further, the chronic oxidative stress of cardiac myocytes can lead to CamKII overexpression-related cardiac dysfunction [5]. Accordingly, monitoring OxyMb, DeoxyMb or the mechanisms by which *met*Mb is formed and reduced in normoxia and hypoxia is a promising field of research. Future studies with this novel *met*Mb/O_2 sensor may provide insight into the functional roles of *met*Mb at the cellular level, which were limited prior to the development of this probe.

Tissue-block level studies previously available for myoglobin status are certainly valuable, but the opportunity to explore mosaic behavior at the cell (or even subcellular) level may be fruitful. Overall, EYFP-Myoglobin-mCherry (or its individual paired protein constituents, for those that do not need all the combined functionality we showed here) can provide valuable views of intracellular distribution and regulation of O_2, ROS and NO. We hope multiphoton microscopic studies of these molecular species in variegated tissues *in vivo* will soon follow.

Supplementary Material

Refer to Web version on PubMed Central for supplementary material.

ACKNOWLEDGMENTS

This work was supported by the Intramural Research Program of the National Heart, Lung, and Blood Institute (NHLBI), and the Eunice Kennedy Shriver National Institute of Child Health and Human Development (NICHD), National Institutes of Health (NIH). We would like to acknowledge Dr. Timothy C. Zhu from the University of Pennsylvania, School of Medicine, Department of Radiation Oncology for providing TOOKAD photosensitizer. We thank the Light Microscopy Core at NHLBI (esp. Dr. Christian Combs) for helpful discussions and the use of their confocal microscopes for fluorescence intensity measurements. We thank Drs. Ju-Gyeong Kang, Jay H. Chung, Jeonghan Kim, and Shutong Yang of NHLBI and George Patterson of NIBIB for assistance in designing and preparing EYFP construct and different plasmids for our various chimeric sensors.

REFERENCES

[1]. Tejero J, Shiva S, Gladwin MT, Physiol Rev 2019, 99, 311–379. [PubMed: 30379623]

[2]. Shiva S, Huang Z, Grubina R, Sun J, Ringwood LA, MacArthur PH, Xu X, Murphy E, Darley-Usmar VM, Gladwin MT, Circ Res 2007, 100, 654–661. [PubMed: 17293481]

[3]. Chen R, Lai UH, Zhu L, Singh A, Ahmed M, Forsyth NR, Frontiers in Cell and Developmental Biology 2018, 6. [PubMed: 29459892]

[4]. Bell EL, Klimova TA, Eisenbart J, Schumacker PT, Chandel NS, Molecular and Cellular Biology 2007, 27, 5737–5745. [PubMed: 17562866]

[5]. Konstantinidis K, Bezzerides VJ, Lai L, Isbell HM, Wei AC, Wu Y, Viswanathan MC, Blum ID, Granger JM, Heims-Waldron D, Zhang D, Luczak ED, Murphy KR, Lu F, Gratz DH, Manta B, Wang Q, Wang Q, Kolodkin AL, Gladyshev VN, Hund TJ, Pu WT, Wu MN, Cammarato A, Bianchet MA, Shea MA, Levine RL, Anderson ME, J Clin Invest 2020, 130, 4663–4678. [PubMed: 32749237]

[6]. Jansson EA, Huang L, Malkey R, Govoni M, Nihlen C, Olsson A, Stensdotter M, Petersson J, Holm L, Weitzberg E, Lundberg JO, Nat Chem Biol 2008, 4, 411–417. [PubMed: 18516050]

[7]. Penjweini R, Roarke B, Alspaugh G, Gevorgyan A, Andreoni A, Pasut A, Sackett DL, Knutson JR, Redox Biol 2020, 34, 101549. [PubMed: 32403080]

[8]. Penjweini R, Andreoni A, Rosales T, Kim J, Brenner MD, Sackett DL, Chung JH, Knutson JR, J Biomed Opt 2018, 23, 1–14.

[9]. Wu B, Chen Y, Muller JD, Biophys J 2009, 96, 2391–2404. [PubMed: 19289064]

[10]. Hagler L, Coppes RI Jr., Herman RH, J Biol Chem 1979, 254, 6505–6514. [PubMed: 447731]

[11]. Belskie KM, Van Buiten CB, Ramanathan R, Mancini RA, Meat Sci 2015, 105, 89–92. [PubMed: 25828162]

[12]. Flogel U, Fago A, Rassaf T, J Exp Biol 2010, 213, 2726–2733. [PubMed: 20675541]

[13]. Plotnikov EY, Chupyrkina AA, Pevzner IB, Isaev NK, Zorov DB, Biochim Biophys Acta 2009, 1792, 796–803. [PubMed: 19545623]

[14]. Yi J, Heinecke J, Tan H, Ford PC, Richter-Addo GB, J Am Chem Soc 2009, 131, 18119–18128. [PubMed: 19924902]

[15]. Wu LB, Yuan H, Gao SQ, You Y, Nie CM, Wen GB, Lin YW, Tan X, Nitric Oxide 2016, 57, 21–29. [PubMed: 27108710]

[16]. Arihara K, Cassens RG, Greaser ML, Luchansky JB, Mozdziak PE, Meat Sci 1995, 39, 205–213. [PubMed: 22059826]

[17]. Bowen WJ, J Biol Chem 1949, 179, 235–245. [PubMed: 18119239]

[18]. Tofani L, Feis A, Snoke RE, Berti D, Baglioni P, Smulevich G, Biophys J 2004, 87, 1186–1195. [PubMed: 15298921]

[19]. Bunt G, Wouters FS, Biophys Rev 2017, 9, 119–129. [PubMed: 28424742]

[20]. Muller SM, Galliardt H, Schneider J, Barisas BG, Seidel T, Front Plant Sci 2013, 4, 413. 10.3389/fpls.2013.00413. [PubMed: 24194740]

[21]. Levchenko SM, Pliss A, Qu J, Journal of Innovative Optical Health Sciences 2018, 11, 1730009.

[22]. Bajar BT, Wang ES, Zhang S, Lin MZ, Chu J, Sensors (Basel) 2016, 16.

[23]. Balleza E, Kim JM, Cluzel P, Nat Methods 2018, 15, 47–51. [PubMed: 29320486]

[24]. Chen X, Zaro JL, Shen WC, Adv Drug Deliv Rev 2013, 65, 1357–1369. [PubMed: 23026637]

[25]. Carpenter AE, Jones TR, Lamprecht MR, Clarke C, Kang IH, Friman O, Guertin DA, Chang JH, Lindquist RA, Moffat J, Golland P, Sabatini DM, Genome Biol 2006, 7, R100. [PubMed: 17076895]

[26]. Burrow JW, Koch JA, Chuang HH, Zhong W, Dean DD, Sylvia VL, J Surg Res 2007, 140, 90–98. [PubMed: 17418871]

[27]. Lee E, Kariya K, FEBS Letters 1986, 209, 49–51. 10.1016/0014-5793(86)81082-1. [PubMed: 3803575]

[28]. Tamarit J, de Hoogh A, Obis E, Alsina D, Cabiscol E, Ros J, J Proteomics 2012, 75, 3778–3788. [PubMed: 22579746]

[29]. Brzostowski J, Haewon S, Confocal Microscopy: Methods and Protocols (Methods in Molecular Biology), Humana Pr Inc, NY, 2021, pp 315–337.

[30]. Gangwar A, Paul S, Ahmad Y, Bhargava K, Biochimie 2018, 148, 127–138. [PubMed: 29571702]

[31]. Jung T, Engels M, Klotz LO, Kroncke KD, Grune T, Free Radic Biol Med 2007, 42, 773–786. [PubMed: 17320760]

[32]. Livingston DJ, McLachlan SJ, La Mar GN, Brown WD, J Biol Chem 1985, 260, 15699–15707. [PubMed: 4066692]

[33]. Zhu H, Qiu H, Yoon HW, Huang S, Bunn HF, Proc Natl Acad Sci U S A 1999, 96, 14742–14747. [PubMed: 10611283]

[34]. Rapozzi V, Varchi G, Della Pietra E, Ferroni C, Xodo LE, Invest New Drugs 2017, 35, 115–123. [PubMed: 27726093]

[35]. Scherz A, Salomon Y, The Story of Tookad: From Bench to Bedside, Handbook of photomedicine, CRC Press, 2013.

[36]. Papuc C, Goran GV, Predescu CN, Nicorescu V, Comprehensive Reviews in Food Science and Food Safety 2017, 16, 96–123. [PubMed: 33371549]

[37]. Tajima G, Shikama K, Int J Biochem 1993, 25, 101–105. [PubMed: 8432378]

[38]. Wazawa T, Matsuoka A, Tajima G, Sugawara Y, Nakamura K, Shikama K, Biophys J 1992, 63, 544–550. [PubMed: 1420896]

[39]. Yan DJ, Li W, Xiang Y, Wen GB, Lin YW, Tan X, Chembiochem 2015, 16, 47–50. [PubMed: 25392956]

[40]. Hyun DH, Lee GH, Age (Dordr) 2015, 37, 122. [PubMed: 26611738]

[41]. Flonta SE, Arena S, Pisacane A, Michieli P, Bardelli A, Am J Pathol 2009, 175, 201–206. [PubMed: 19541931]

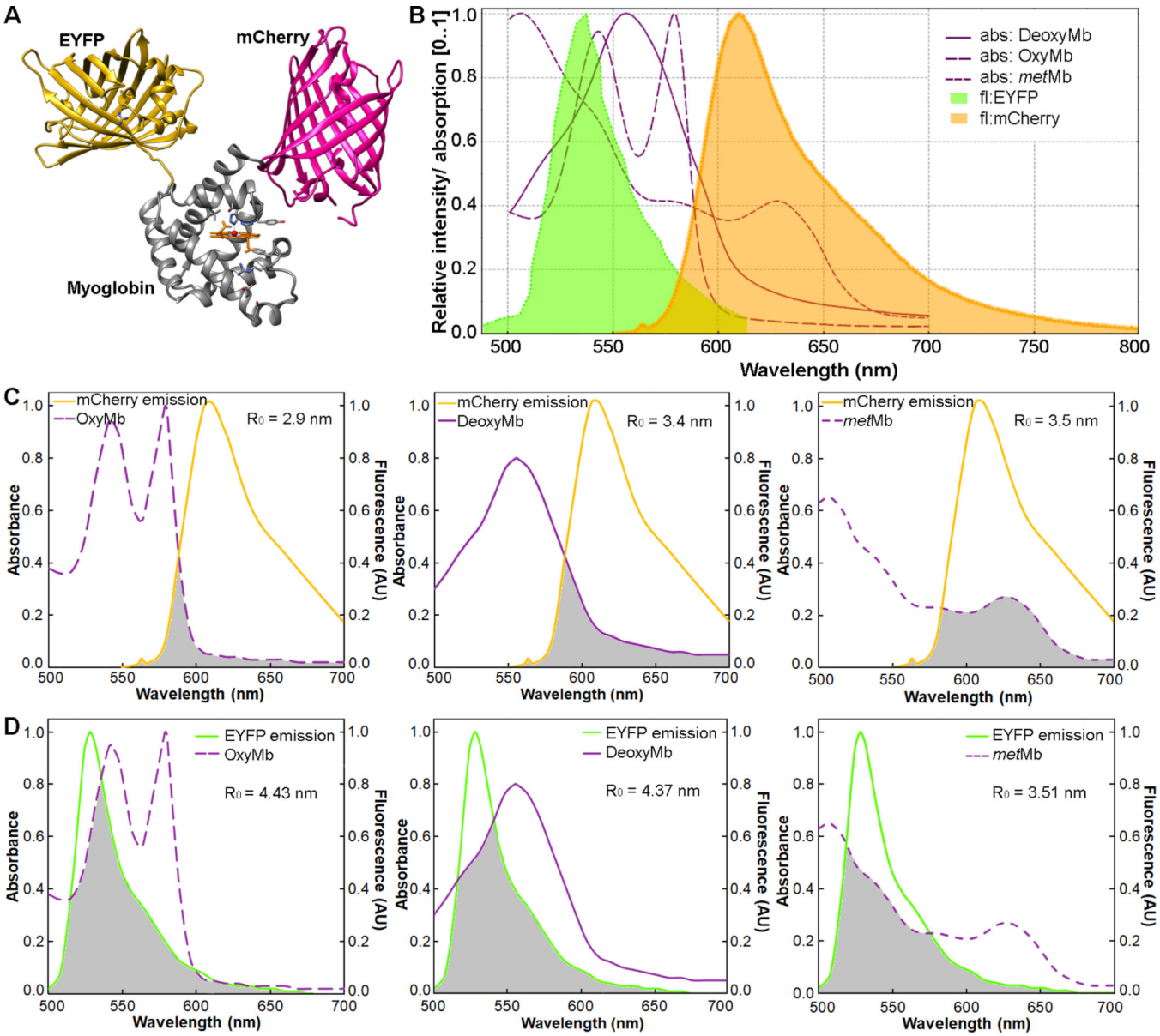

FIGURE 1.

A, Artist's rendering of the EYFP-Myoglobin-mCherry, in which EYFP and mCherry are coupled to the N and C terminus of myoglobin, respectively. B, Absorption spectra of oxygenated (OxyMb), deoxy-genated (DeoxyMb) and *met* (*met*Mb) myoglobin, overlapped with the emission spectra of EYFP and mCherry. C, Absorption spectra of OxyMb, DeoxyMb and *met*Mb overlapped with the mCherry emission to highlight the spectral overlap (a calculation occurring in shaded area) between the species. D, Absorption spectra of OxyMb, DeoxyMb and *met*Mb overlapped with the EYFP emission (shaded area). R_0 is the Förster radius.

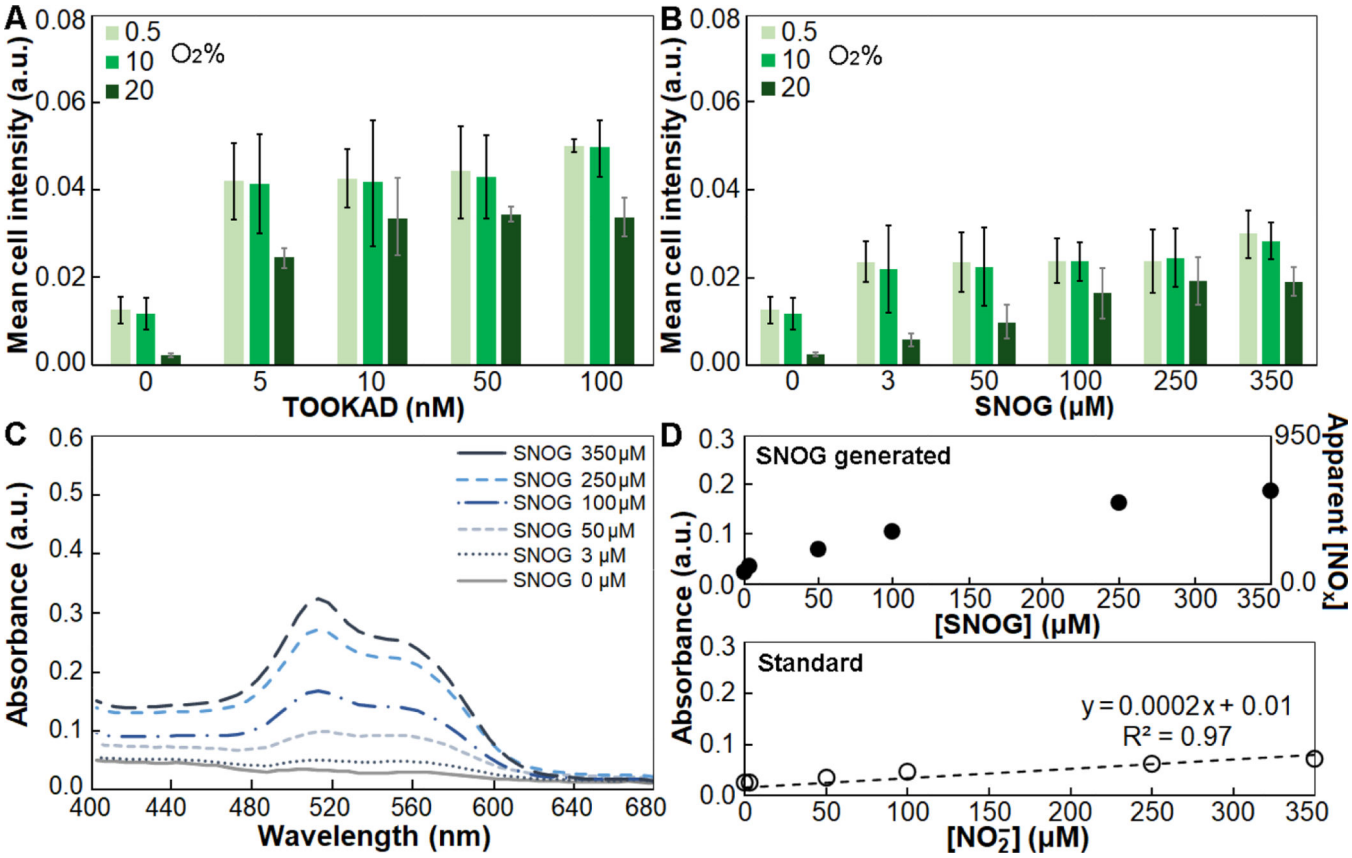

FIGURE 2.

Detection of carbonyl groups with fluorescence imaging of BODIPY FL Hydrazide in A549 cells treated with A, TOOKAD and B, SNOG as compared to the cells with no imposed oxidative stress. The data are presented for O_2% of 20, 10 and 0.5 and error bars are the standard error of the mean. C, Griess assay for NO detection in the cell media with various SNOG concentrations at O_2= 20%. D, SNOG induced absorbance curve (black circles) referenced to the Griess nitrite standard curve (empty circles with dashed black line).

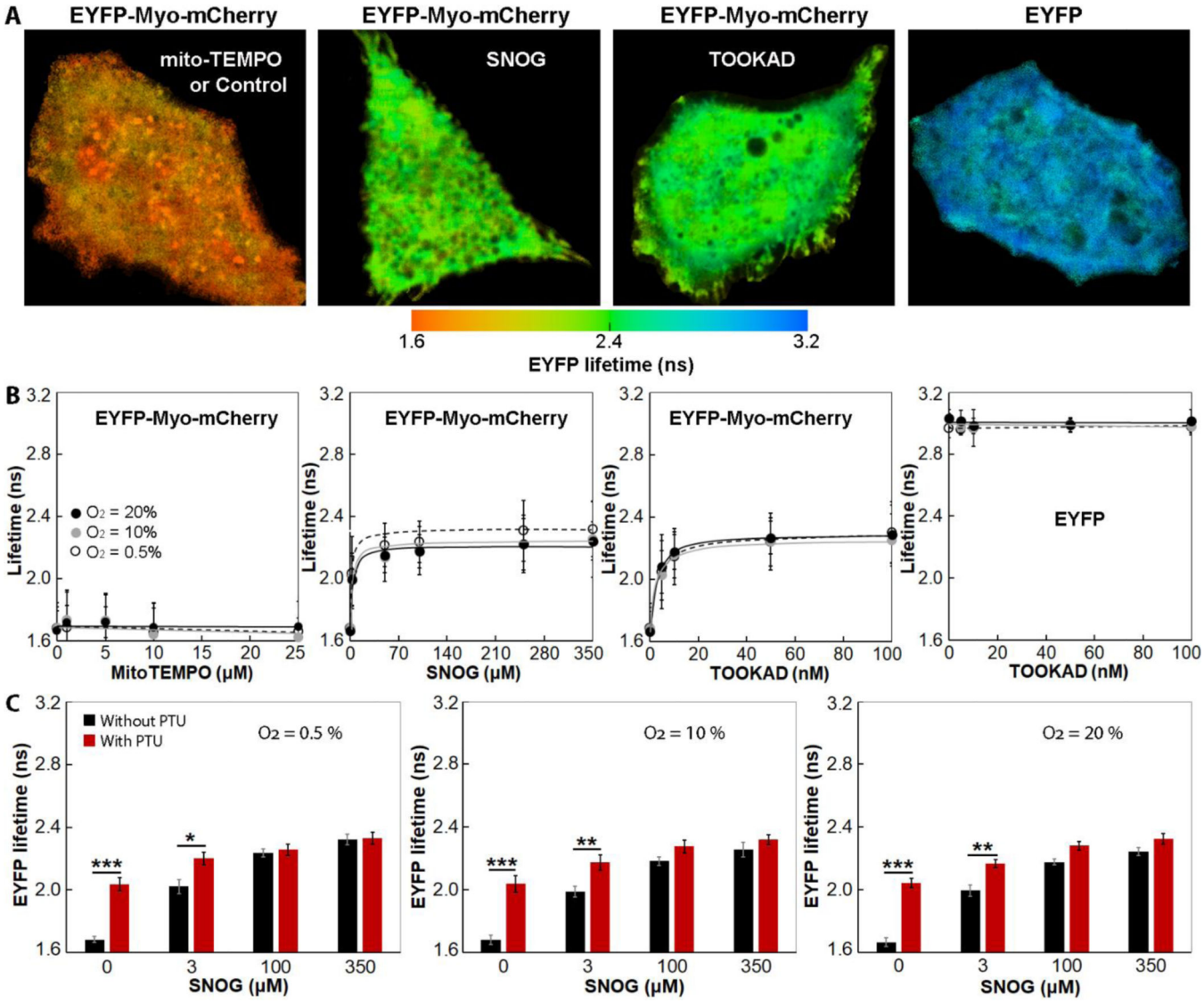

FIGURE 3.

A, From left to right, pseudocolor mapping of EYFP fluorescence lifetime in the FRET sensor (EYFP-Myoglobin-mCherry) and alone in A549 cells treated with 25 μM mito-TEMPO, 350 μM SNOG and 100 nM TOOKAD. B, Changes of the average lifetime of EYFP in the FRET sensor vs. mito-TEMPO, SNOG and TOOKAD concentration at various imposed O_2%. The average lifetime of EYFP (alone) vs. mito-TEMPO, SNOG and TOOKAD concentrations did not change- example in right panel. C, Changes of the average lifetime of EYFP in the FRET sensor in response to the SNOG treatment and inhibition of cytochrome b_5 reductase using propylthiouracil (PTU). The error bars are standard error of the mean calculated from at least 30 cells. Note the earlier detection of *met*Mb when PTU blocks reductase.

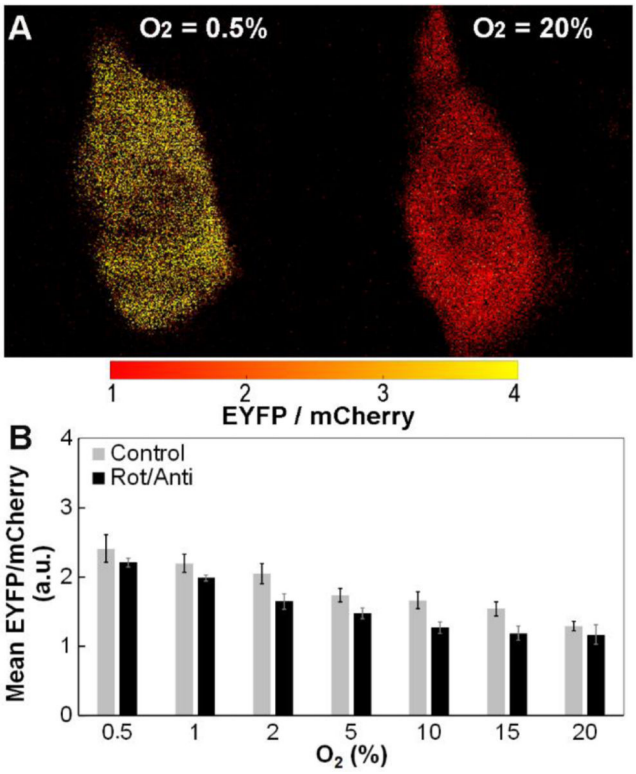

FIGURE 4.

A, Pseudocolor mapping of the EYFP/mCherry intensity ratio in the intracellular environment of A549 cells in response to normoxia (O_2 = 20%) and anoxia (O_2 = 0.5 %); yellow and red indicate larger and smaller ratio, respectively. B, The changes of EYFP/mCherry intensity ratio in response to different imposed O_2% from 20 to 0.5. The error bars are the standard error of the mean from at least 30 cells. Note that inhibited cells have reduced internal O_2 sinks and hence show lower ratios appropriate for higher internal [O_2].